^{18}F-FDG microPET imaging differentiates between septic and aseptic wound healing after orthopedic implant placement

A longitudinal study of an implant osteomyelitis in the rabbit tibia

Jim C E Odekerken[1], Boudewijn T Brans[2], Tim J M Welting[1]*, and Geert H I M Walenkamp[1]*

[1]Laboratory for Experimental Orthopaedics, Department of Orthopaedic Surgery, CAPHRI School for Public Health and Primary Care; [2]Department of Nuclear Medicine, Maastricht University Medical Center, Maastricht, the Netherlands.
Correspondence: jim.odekerken@maastrichtuniversity.nl
*These authors contributed equally.
Submitted 13-07-30. Accepted 14-01-24

Background and purpose — ^{18}F-FDG PET is a widely used tool for molecular imaging of oncological, cardiovascular, and neurological disorders. We evaluated ^{18}F-FDG microPET as an implant osteomyelitis imaging tool using a *Staphylococcus aureus*-induced peroperative implant infection in rabbits.

Methods — Intramedullary titanium nails were implanted in contaminated and uncontaminated (control) proximal right tibiae of rabbits. Tibiae were quantitatively assessed with microPET for ^{18}F-FDG uptake before and sequentially at 1, 3, and 6 weeks after surgery. Tracer uptake was assessed in soft tissue and bone in both treatment groups with an additional comparison between the operated and unoperated limb. MicroPET analysis was combined with radiographic assessment and complementary histology of the tibiae.

Results — At the first postoperative week, the ^{18}F-FDG uptake in the contaminated implant group was significantly higher than the preoperative measurement, without a significant difference between the contaminated and uncontaminated tibiae. From the third postoperative week onward, ^{18}F-FDG uptake allowed discrimination between osteomyelitis and postoperative aseptic bone healing, as well as quantification of the infection at distinct locations around the implant.

Interpretation — ^{18}F-FDG-based microPET imaging allows differentiation between deep infection and undisturbed wound healing after implantation of a titanium intramedullary nail in this rabbit model. Furthermore, our results indicate that ^{18}F-FDG PET may provide a tool in human clinical diagnostics and for the evaluation of antimicrobial strategies in animal models of orthopedic implant infection.

With more prostheses and osteosyntheses being implanted every year and a suggested increase in infection rate, the absolute number of implant infections will increase (Dale et al. 2009, Acklin et al. 2011, Kurtz et al. 2012). Deep orthopedic implant infections are difficult to diagnose in the early postoperative weeks, while diagnosis of infection in this period is important for optimal treatment and implant survival. A specific diagnostic tool to monitor implant infections is therefore imperative.

Current diagnostics to detect orthopedic implant infections are based on clinical symptoms, hematological parameters, radiology, and nuclear scintigraphy. However, as in low-grade infections, in the early postoperative phase changes such as periosteal reactions and cortical thickening (Calhoun and Mader 1997, Smeltzer et al. 1997, Odekerken et al. 2013) or osteolysis and calcifications (Calhoun and Mader 1997, Smeltzer et al. 1997, Vogely et al. 2000, Odekerken et al. 2013) are not specific enough to differentiate between implant/soft tissue infection and aseptic wound problems. More discriminative power is needed to distinguish aseptic wound healing from bacterial infection and to follow implant infection quantitatively over time. ^{18}F-fluorodeoxyglucose (^{18}F-FDG) is widely used as a positron emission tomography (PET) tracer to diagnose and monitor several pathological conditions in the clinic (Stumpe et al. 2000, Toyama et al. 2004a,b, van der Bruggen et al. 2010, Huang et al. 2012, Marsboom et al. 2012). The use of ^{18}F-FDG as a tracer is based on a local increase in metabolic turnover of glucose. Since the presence of bacteria and increased leukocyte infiltration in an infected area generates such a local increase in glucose turnover and leads to increased ^{18}F-FDG uptake (Stumpe et al. 2000, Koort

DOI 10.3109/17453674.2014.900894

et al. 2004, Makinen et al. 2005a), local detection of bacterial infections is possible.

We hypothesized that ^{18}F-FDG PET scanning would be capable of providing the discriminative power needed to distinguish aseptic wound healing from orthopedic implant infection. To test this hypothesis, we sequentially determined the development of implant osteomyelitis by ^{18}F-FDG microPET scanning of contaminated and uncontaminated rabbit tibiae and explored its possible use in diagnosis of implant infection.

Materials and methods

Experimental group

22 specified pathogen-free (SPF) female New Zealand White (NZW) rabbits (Charles River, Chatillon-sur-Chalaronne, France), each weighing 3.5–4 kg, were used in this study. They were allowed to acclimatize for 2 weeks before the start of the experiments. 13 animals, randomly chosen from the population, were scanned with F-FDG microPET two weeks before surgery to define the background tracer uptake level in a healthy animal without surgical intervention. On the day of surgery, the population was subdivided into 2 equal-sized, randomly assigned groups: an uncontaminated implant group (sterile saline control) and a contaminated implant group.

Anaesthesia was initiated by ketamine (35 mg/kg i.m.) and xylazine (5 mg/kg i.m.), while maintained by fentanyl (2 µg/kg/h i.v.), midazolam (1 mg/kg/h i.v.) and if necessary supported by isoflurane (1%). A 2% iodine solution in ethanol was used for the disinfection of the shaved right hind leg of the animal.

A transpatellar incision was made to gain access to the tibial plateau. A 4-mm-wide opening was drilled, by sequential reaming, with a hand drill into the tibial plateau to gain access to the intramedullary cavity. Residual bone fragments and hematoma were removed by irrigation. Each animal received a 4-mm-wide, 20-mm-long, grit-blasted titanium alloy (TiAl6V4) implant (DePuy; Johnson and Johnson, UK) into the tibial intramedullary cavity.

The uncontaminated implant group received a 100-µL sterile saline injection into the intramedullary cavity before placing of the titanium implant. The implant infection group received a single dose of on average 3.8 × 105 colony-forming units (CFU) Staphyloccocus aureus (UAMS-1; ATCC 49230) in 100 µL saline, into the intramedullary cavity before implantation. The implant was positioned distal to the tibial articulating surface. The bone defect was sealed with bone wax (Syneture; Covidien, Mansfield, MA) and the surrounding soft tissues were flushed with sterile saline. The wound was closed in layers with single resorbable sutures and protected by application of "Aluminum Spray" (Eurovet Animal Health, Bladel, the Netherlands).

The rabbits were housed in groups to stimulate physical activity and therefore movement of the operated leg. They were randomly assigned to a housing group based on the day of surgery, resulting in mixed housing of animals with contaminated and uncontaminated implants. Animals received food and water ad libitum; their daily diet was supplemented with 20 g "Critical Care" (Oxbow Animal Health, Murdock, NE) to maintain their physical condition. The animals were checked on a daily basis for general health and experiment-related discomfort over a period of 6 weeks. Pain treatment by injection of buprenorphine (0.05 mg/kg body weight) was given twice a day for the first 2 days after surgery, and continued if pain persisted.

Tibial fracture, sepsis, and extensive formation of soft tissue abscesses and fistulae were defined as humane endpoints in accordance with the directions of the institutional animal ethics committee. Where there was 20% weight loss, a veterinarian was consulted and the rabbit was either treated with additional individual feeding with "Critical Care" or it was killed. All remaining animals were sacrificed 6 weeks after surgery with an overdose of pentobarbital (Euthanimal; Alfasan, Woerden, the Netherlands).

The study was approved in September 2010 by the Maastricht University Animal Ethics Committee (DEC-UM protocol 2010-089).

Radiographic imaging

To assess bone quality and implant positioning, radiographs were taken under tiletamine-zolazepam anesthesia (15 mg/kg body weight) at weekly intervals, starting immediately after surgery. Anteroposterior and lateral images were acquired at 85 kV and 20 mAs (Polymobil; Siemens, Germany) on Kodak PQ-phosphor screens (Carestream Health, Rochester, NY). The radiographs were digitized using a CR-975 phosphor screen reader (Carestream Health) and visualized with the Philips iSite software package version 3.5. Radiographs were assessed for signs of osteomyelitis (periosteal elevation, cortical thickening, and osteolysis) (Calhoun and Mader 1997, Odekerken et al. 2013).

After 6 weeks of follow-up, the animals were killed and the hind leg was excised in a sterile fashion. Ex vivo micro-CT imaging of these excised hind legs was performed directly after death. Images were acquired on an X-rad 225 (Precision X-ray, North Branford, CT), with a field of view 10 cm in diameter, a source-to-axis distance of 30 cm, and a source-to-detector distance of 62 cm. Images were acquired at 80 kVp, with an isotropic spacing of 102 µm and 2.14 mm AI added filtration. The GE MicroView software package version 2.1.2 (GE Healthcare) was used for the image evaluation.

^{18}F-FDG microPET imaging

The microPET scans of the rabbit hind legs were performed on a Focus 120 microPET scanner (Siemens, Germany) (Figure 1). The entire microPET procedure, lasting approximately 2 h, was performed under tilatamine-zolazepam sedation, which was initiated with a 15 mg/kg intramuscular dose and fol-

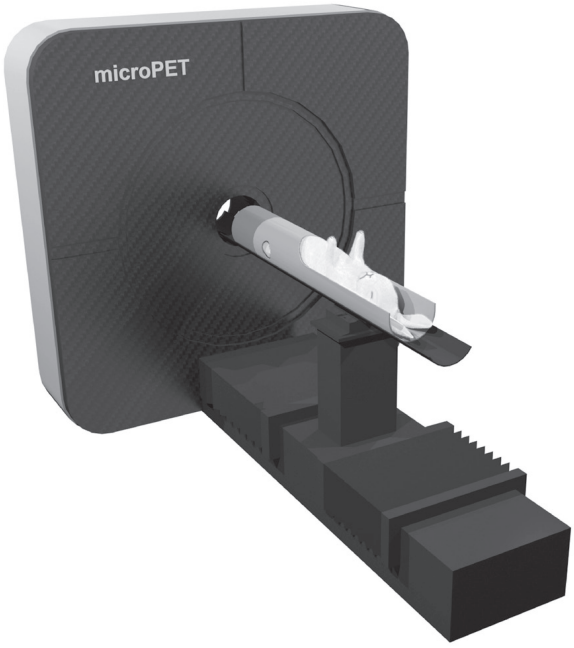

Figure 1. Diagram of the experimental setup. Positioning of a rabbit in the custom-made restrainer on the Siemens Focus 120 microPET scanner.

lowed with 3 additional intramuscular injections of 7.5 mg/kg. A preoperative scan and 3 postoperative scans (at 1, 3, and 6 weeks after surgery) were acquired to assess the progress of implant infection in each animal. The rabbits were placed in a custom-made PVC restrainer (Figure 1), which allowed the rabbit to breath freely without allowing any movement of the hind legs. 50 MBq ^{18}F-FDG (GE Healthcare Medical Diagnostics, Eindhoven, the Netherlands) was diluted with sterile saline to a volume of 1 mL and subsequently injected in the ear vein of the rabbit. A 1-h incubation period was taken into account to allow uptake of the ^{18}F-FDG in the area of interest.

Acquired data were reconstructed iteratively in a 128 × 128 × 95 matrix using attenuation-weighed 2-dimensional ordered-subsets expected maximization (OSEM2D). The spatial resolution of the microPET scans was 1.4 mm at the center of the field of view.

Data were analyzed with the ASIPRO VM software package version 6.7.1.2 (Concorde Microsystems; Siemens, Germany). A cylindrical VOI of 10.4 mm in diameter and 25.1 mm long was used as a contour around the implant and the surrounding bony tissue. An equal-sized VOI was placed in the contralateral leg at an equivalent location to where the implant was placed in the experimental leg. Each leg also contained an equal-sized VOI in the vastus lateralis to serve as a measurement of soft tissue uptake of ^{18}F-FDG. In addition, 3 circular ROI (10.4 mm in diameter and 0.87 mm in thickness) were constructed at the proximal, central, and distal part of each implant. The standardized uptake value (SUV) was calculated from the total activity in the selected ROI and VOI, corrected for the weight of the animal and the activity of ^{18}F-FDG in the animal at the time of emission scanning. Activity at the time of the scan was corrected for the activity injected and the calibration factor of the microPET and dose calibrator (CRC 25R; Capintec Inc., Ramsey, NJ).

Quantification of infection

Weekly assessments of clinical, hematological, and radiographic infection parameters, combined with post-mortem micro-CT, were performed to confirm the absence or presence of an infection in the uncontaminated and contaminated implants. Also, post-mortem bone tissue culture was performed to verify the presence of bacteria. Bacterial growth was assessed on tellurite glycine agar after 24 h of culture. After sampling for bacterial culture, the remaining part of the tibia, which included the implant, was fixed in a 4% formaldehyde/PBS solution for 4 weeks, followed by alcohol dehydration and embedding in polymethylmethacrylate (PMMA) (Technovit 9100; Hereaus Kulzer, Germany). Once polymerized, 50-µm sections were acquired on a saw microtome (SP 1600; Leica, Germany), stained according to Masson-Goldner (Carl Roth, Germany) or Gram, and glued onto a microscope slide with UV-polymerizing glue (Permacol B.V., Ede, the Netherlands). The sections were viewed with light microscopy and digital images were taken (Axioscope A1; Axiovison LE release 4.8.2; Carl Zeiss, Germany). The images acquired were fused using Photoshop CS3 software (Adobe Systems) to generate overview images.

Statistics

Significant differences between the contaminated and uncontaminated implant groups were determined using Student's t-test for independent samples. Significant differences between the operated and unoperated contralateral legs were determined with a paired-samples t-test. Statistical significance was assumed for p-values of ≤ 0.05.

Statistical analysis was performed with SPSS software version 21. Graphical representation of the statistical data was performed with GraphPad Prism 5.

Results

The animals with an uncontaminated implant recovered to full weight bearing within the first 2 weeks after surgery, while in the contaminated implant group the animals only showed partial weight bearing of the operated leg throughout the experiment. From 22 animals initially, 3 animals did not recover from anesthesia and 3 other animals (all in the contaminated implant group) had to be killed before the end of the study because of humane endpoints related to the bacterial infection. Furthermore, the use of tiletamine-zolazepam for anesthesia caused muscle contractions in 1 animal, which could

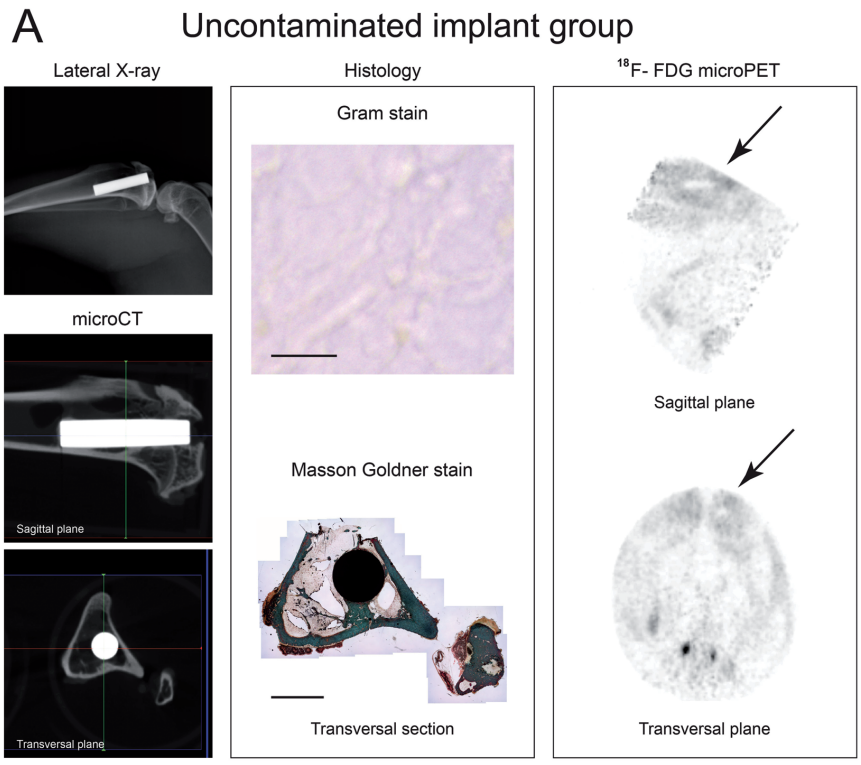

Figure 2. Results of radiology, histology, and microPET 6 weeks after surgery. A. Uncontaminated implant group. The lateral X-ray (upper left panel) shows normal bone morphology. Micro-CT images (the 2 lower left panels) indicate a healthy cortex with bone apposition on the implant surface. Transversal micro-CT corresponds to the transversal histology section (lower image in middle panel; bar represents 4 mm), which indicates bone apposition on the implant and normal bone morphology. Absence of Gram-positive bacteria confirmed the absence of infection (upper image in middle panel; bar represents 20 µm). Reconstructed ^{18}F-FDG microPET planes (right panel) indicate tracer uptake and implant location (arrows). B. Contaminated implant group. Lateral X-ray (upper left panel) indicates cortical thickening and osteolysis. Micro-CT (the 2 lower left panels) supports the findings on X-ray images, with cortical thickening and extensive osteolysis. Transversal micro-CT corresponds to the transversal histology section (lower middle panel; bar represents 4 mm), additionally indicating the presence of an intramedullary abscess. The presence of Gram-positive bacteria confirmed the presence of a bacterial infection (upper middle panel; bar represents 20 µm). Reconstructed ^{18}F-FDG microPET planes (right panel) indicate implant location and increased tracer uptake (arrows).

not therefore be scanned on the microPET at all time points. Complete datasets were acquired from 8 animals with an uncontaminated implant and from 7 animals with a contaminated implant. Datasets from animals that did not complete the experimental follow-up were excluded from the data analysis.

Infection status

We first determined whether there was development of infection. The experimental procedure resulted in initial weight loss during the first postoperative weeks in all animals. Only the uncontaminated control group recovered to their preoperative weight within 4 weeks, while animals in the contaminated implant group remained below their preoperative weight. Erythrocyte sedimentation rate (ESR) and C-reactive protein (CRP) were elevated in the contaminated implant group (supplementary Figure 1). During the 6-week follow-up, the severity of the radiographic signs of osteomyelitis (periosteal elevation, cortical thickening, and osteolysis) increased in the contaminated implant group. In the uncontaminated control group, radiographic signs of osteomyelitis were absent (Figure 2). Post-mortem micro-CT imaging of the operated tibiae confirmed the radiographic findings, especially in the group with contaminated implants (Figure 2B). Bone apposition on the implant surface was detected in the uncontaminated implant group (Figure 2A) but not in the contaminated implant group (Figure 2B).

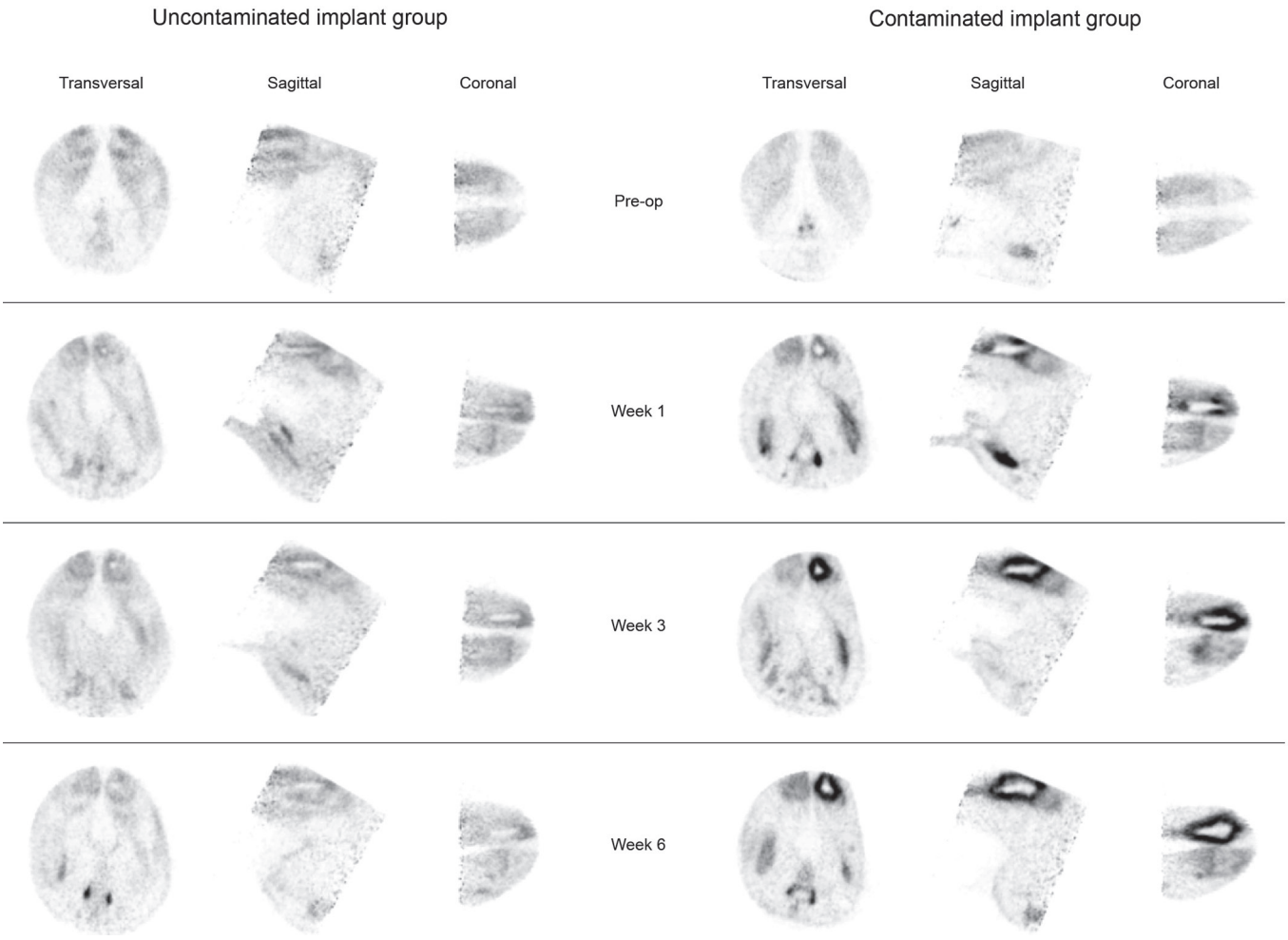

Figure 3. Representative images of ^{18}F-FDG uptake in the uncontaminated implant group (left) and the contaminated implant group (right) during the 6-week follow-up.

Bacterial culture of the peri-implant tissue on tellurite glycine agar showed S. aureus culture positivity in 6 out of 7 contaminated implants, while none of the uncontaminated implants were culture-positive for *S. aureus*.

Microscopic analysis of the histological sections showed a clear difference between the uncontaminated implant group and the contaminated implant group. Undisturbed cortex integrity was observed in the uncontaminated implant group, with bone apposition on the implant surface. In sharp contrast, the contaminated implant group showed cortical thickening, abscess formation, and osteolysis around the implant. Gram staining of similar sections showed the presence of Gram-positive cocci in the contaminated implant group (Figure 2). Overall, these data confirm that the uncontaminated group did not develop an osteomyelitis, whereas the contaminated group showed all signs of an implant infection leading to osteomyelitis.

^{18}F-FDG uptake in bone and soft tissue around the implant

OSEM2D reconstructed microPET images of the contaminated implant group indicated that the ^{18}F-FDG uptake was localized in the morphologically affected bone tissue (according to radiographs, micro-CT, and histology) (Figure 2B). Furthermore, the reconstructed images from the implant infection group showed higher ^{18}F-FDG uptake around the implants than in the uncontaminated implant group throughout the experimental follow-up (Figure 3).

To quantify the ^{18}F-FDG uptake in both groups and investigate whether ^{18}F-FDG microPET enables differentiation between control and infected implants, the ^{18}F-FDG uptake by the soft tissues and also the uptake by the bone tissue around the implants was determined separately and compared. Throughout the entire follow-up, quantification of ^{18}F-FDG uptake in the soft tissues (vastus lateralis) of the uncontaminated control group showed similar uptake in the soft tissue of

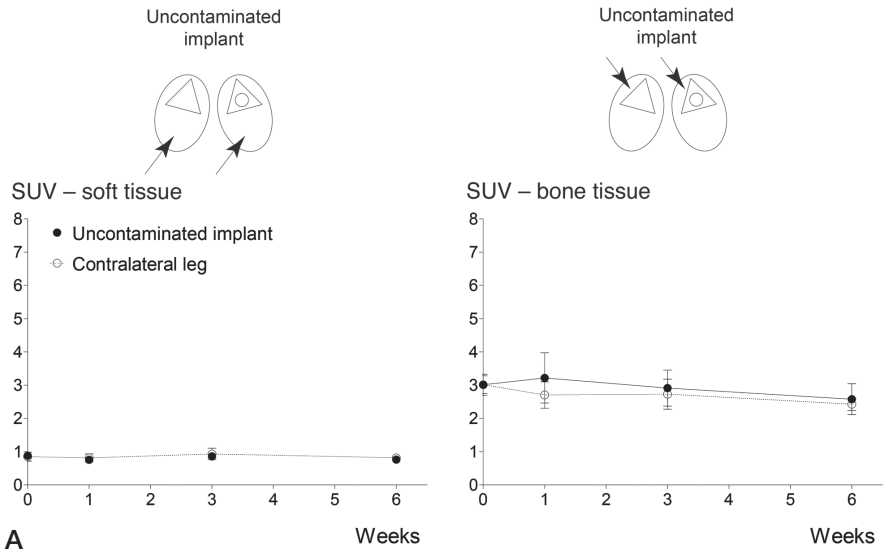

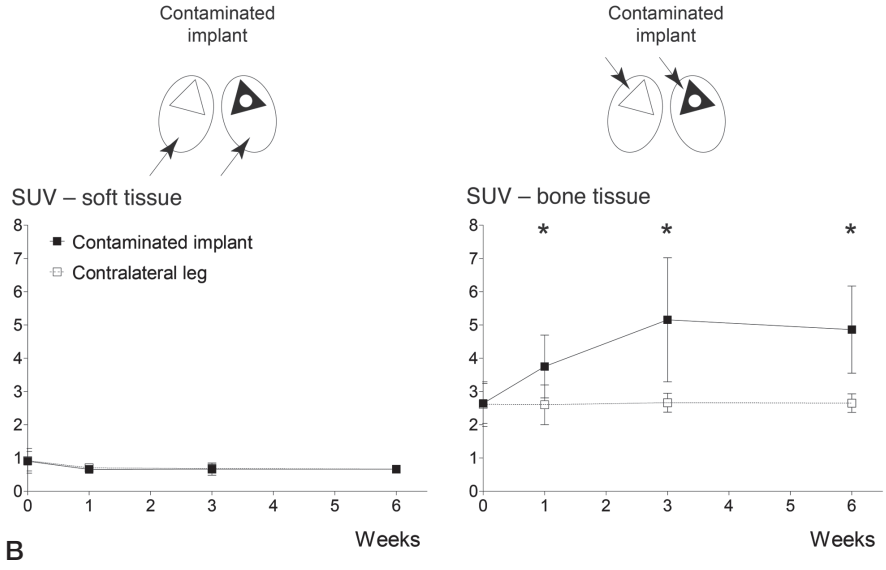

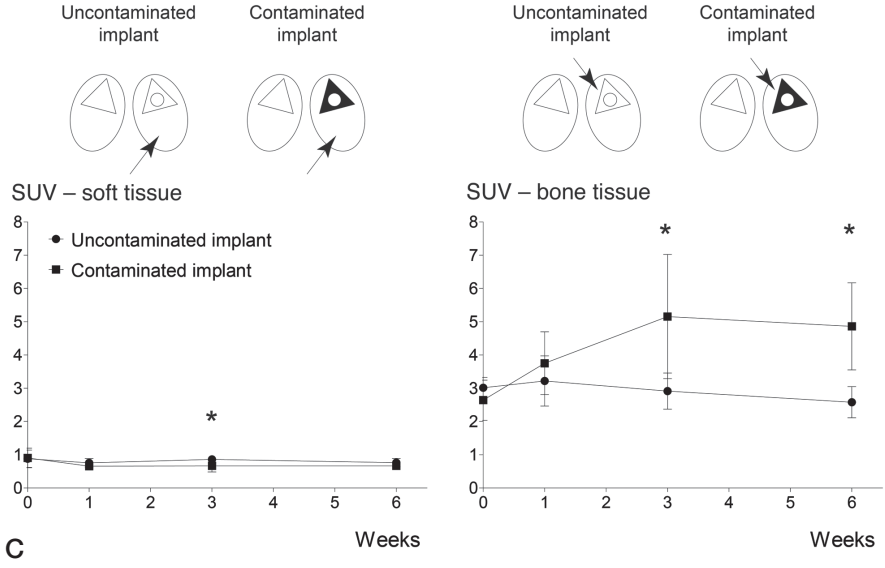

the tibia containing an implant to that in the unoperated contralateral tibia of the same animal (Figure 4A, left panel). The uptake of ^{18}F-FDG by the bone tissue surrounding the uncontaminated implant was compared to the uptake in the same region of the contralateral unoperated tibia. A borderline statistically significant difference between SUVs from both regions was found after the first postoperative week only (Figure 4A, right panel) (week 0: p = 1.0; week 1: p = 0.05; week 3: p = 0.5; and week 6: p = 0.4). The soft tissues in the contaminated implant group showed similar ^{18}F-FDG uptake between the operated and unoperated tibia at all time points (Figure 4B, left panel). In contrast, the bone tissue surrounding the contaminated implant showed a significantly higher uptake of ^{18}F-FDG than was found in the same region in the unoperated contralateral tibia at all 3 postoperative time points (Figure 4B, right panel) (week 0: p = 0.6; week 1: p = 0.002; week 3: p = 0.01; and week 6: p = 0.005). The soft tissue uptake in the uncontaminated group showed a minimal, but significantly higher uptake than the soft tissue in the contaminated implant group (p = 0.05) at 3 weeks only (Figure 4C, left panel). The ^{18}F-FDG uptake in the bone surrounding the implant showed a significantly higher uptake in the contaminated implant group than in the uncontaminated implant group in the third and

Figure 4. Quantification of the uptake of ^{18}F-FDG tracer. Illustrations above the graphs are schematic representations of a transverse section of the rabbits' hind legs, with the implant-containing tibia on the right (ellipsoids represent the soft tissues, triangles represent the tibiae (with black triangles representing the contaminated tibiae), and circles represent the implants). Black arrows indicate the tissues compared in the corresponding graph. A. Uncontaminated implant group. Quantification of the tracer uptake in soft tissue (left panel) and the tracer uptake in both tibiae (right panel). B. Contaminated implant group. Quantification of the tracer uptake in soft tissue (left panel) and the tracer uptake in both tibiae (right panel). C. Comparison of tracer uptake in the operated leg in the uncontaminated group with that in the contaminated implant group. Asterisks indicate p-values < 0.05. The error bars represent 95% confidence intervals.

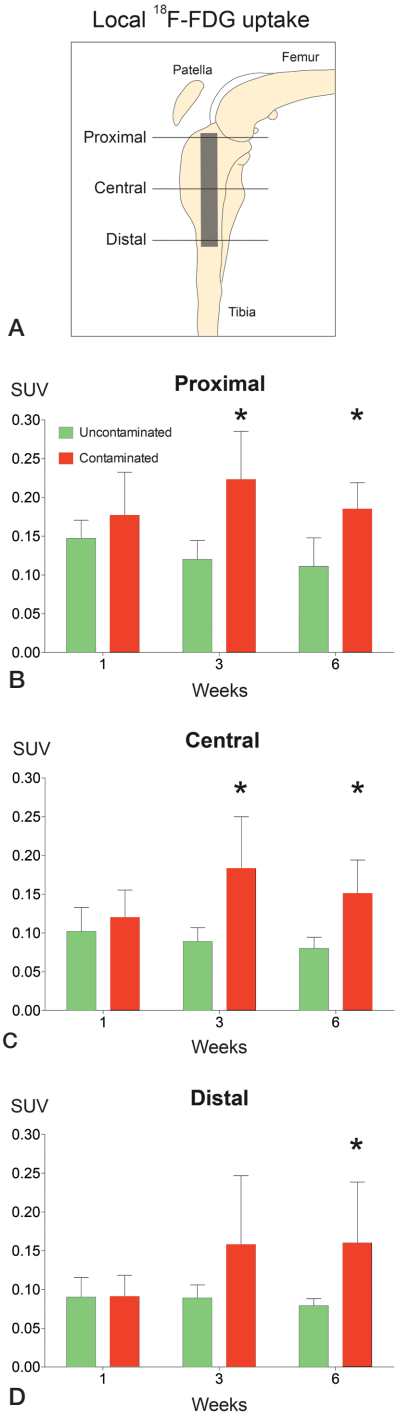

Figure 5. Quantification of localized tracer uptake. A. Graphical representation of the implant positioning and the location of the placed ROI. B–D. Comparisons between the tracer uptake in the uncontaminated implant group and that in the contaminated implant group, based on ROI location. Asterisks indicate $p < 0.05$. The error bars represent 95% confidence intervals.

sixth weeks after surgery (Figure 4C, right panel) (week 3: p = 0.03; week 6: p = 0.004), but not in the first postoperative week (p = 0.3).

To determine whether the magnitude of the infection-associated ^{18}F-FDG signal from the bone surrounding the implants was related to a specific region around the implant, circular regions of interest were placed in the OSEM2D reconstructed microPET images from both groups at positions corresponding to the proximal, central, and distal parts of the implant (Figure 5A). The uptake in bone surrounding the proximal part of the implant was significantly higher in the contaminated implant group than in the uncontaminated implant group in the third and sixth weeks after surgery (Figure 5B) (week 3: p = 0.006; week 6: p = 0.004). Similarly, around the central part of the contaminated implant the uptake was significantly higher than in the uncontaminated implant in the third and sixth postoperative weeks (Figure 5C) (week 3: p = 0.01; week 6: = 0.006). At the distal part of the contaminated implant, the uptake was significantly higher in the sixth postoperative week only (Figure 5D) (p = 0.05).

Discussion

^{18}F-FDG has been suggested as an infection-specific tracer in the field of orthopedics (Guhlmann et al. 1998, Schmitz et al. 2000, Temmerman et al. 2001, Koort et al. 2004, Nanni et al. 2009, Tremoleda et al. 2011). However, most of these studies concentrated specifically on osteomyelitis without implants (Koort et al. 2004, Jones-Jackson et al. 2005, Makinen et al. 2005a). Few other studies have focused on osteomyelitis in connection with the introduction of an antibiotic-containing bioresorbable screw or bone cement (Koort et al. 2005, Makinen et al. 2005b, Lankinen et al. 2012). However, metal implants are the most commonly used orthopedic implants for fracture fixation (nails, screws, and plates) and joint replacement, and they carry the risk of bacterial infection. Surprisingly, no experimental osteomyelitis studies focusing on metal implants and using microPET to quantify the osteomyelitis have been reported. The use of ^{18}F-FDG PET might lead to to earlier diagnosis of infection, with important implications for treatment success and implant survival (Temmerman et al. 2001, De Winter et al. 2002, Zhuang and Alavi 2002, Geurts et al. 2011, 2013).

Experimental models of implant infection generally focus on clinical endpoints rather than imaging endpoints, due to the potential risk of losing animals as a result of the repeated periods of general anesthesia required to obtain imaging data (Lankinen et al. 2012). Rats are not heavily affected by the repeated use of anesthesia and they are more resilient to heavy antibiotic treatment (Mader 1985, Cremieux and Carbon 1997), so this species may be preferable for such studies (Alt et al. 2011). On the other hand, rats need a far higher bacterial dose to achieve a persistent implant infection and the bones of rats are rather small for the study of larger orthopedic implants (Makinen et al. 2005a). Thus, the rabbit has been the preferred species for experimental osteomyelitis studies since the late nineteenth century (Rodet 1973).

In contrast to other authors, we used a microPET scanner that was suitable for small animals instead of a normal PET scanner for patients (Koort et al. 2004, Jones-Jackson et al. 2005, Makinen et al. 2005a, Lankinen et al. 2012). The main reason for not using microPET in previous rabbit studies was the limited size of the gantry of a microPET scanner. Since microPET scanners are mainly meant for experiments with mice and rats, they do not allow positioning of a rabbit without the need for a special fixation device. Our fixation device allowed proper placement of the rabbit during the whole period of the ^{18}F-FDG incubation after injection, and during the microPET scan with the rabbit under anesthesia. In this way, we were able to scan at a higher resolution than the resolution achieved on a conventional clinical PET scanner, thus obtaining a more detailed insight into the location of the ^{18}F-FDG.

Work by Jones-Jackson et al. (2005) showed that in a within-subject longitudinal follow-up in an osteomyelitis model based on the forelimbs of rabbits without any implant, increased FDG uptake could be detected in the first postoperative week. They found a subsequent drop in uptake in the uncontaminated control group in the weeks that followed, while uptake in the infected group continued to increase up to the third postoperative week. Our results are in agreement with this study, and show that also in the presence of an orthopedic titanium implant, the development of an osteomyelitis shows a comparable pattern of uptake of ^{18}F-FDG by the infected bone tissue. In clinical practice, differentiation between the postoperative inflammation and infection-related inflammation is a well-known problem, troubling early infection intervention (Zimmerli and Ochsner 2003, Trampuz and Zimmerli 2006). Our microPET data suggest that there was an aseptic wound healing response in the first postoperative week in the uncontaminated implant group. In our experimental setting, the earliest differentiation between ^{18}F-FDG uptake from aseptic wound healing and septic wound healing was possible from the third postoperative week onwards.

^{18}F-FDG is rather more of a specific tracer for increased metabolic glucose turnover than an infection-specific tracer. However, infection or postoperative tissue healing is related to a locally increased metabolic turnover of glucose. In the case of an infection, this is mainly caused by leucocytes, neutrophilic granulocytes, and macrophages, but also by bacteria present in the infected tissue (Stumpe et al. 2000, Koort et al. 2004, Makinen et al. 2005a, Stumpe and Strobel 2006). Our findings show for the first time that microPET can differentiate aseptic wound healing from septic wound healing in an orthopedic implant animal model using ^{18}F-FDG. As a statistically insignificant postoperative peak in ^{18}F-FDG uptake was found in the first postoperative week in the uncontaminated implant group, whereas the uptake in the contaminated implant group reached its peak in the third postoperative week, this suggests that the most optimal time point to perform the initial imaging in this particular implant model may be during the end of the third postoperative week.

Most of the uptake of ^{18}F-FDG was located at the proximal part of the contaminated implant. This may reflect a more intense local infection. However, as there are differences in bone thickness between the proximal and distal tibiae, this may also indicate that the thickness of the affected epiphyseal and metaphyseal bone tissue in that area contributes to the increase in local FDG uptake observed. Based on our clinical experience in chronic implant infections, the intramedullary abscess would be expected to spread under the influence of gravity to the more distal tibia. We found that the uptake at the distal part of the contaminated implant became higher (compared to the uncontaminated control group) in the sixth postoperative week, supporting this clinical observation. Thus, scanning at later time points in follow-up would be expected to provide more insight into the spread of the infection.

In summary, we found that ^{18}F-FDG can be used as a sensitive postoperative tracer of infection in an *S. aureus*-induced implant infection model in the tibia of the rabbit. From the third postoperative week onward, microPET scanning could differentiate implant infection from aseptic wound healing and bone remodeling. This highlights its potential value in human clinical diagnostics for detection of early postoperative orthopedic infections. Furthermore, our data support the use of ^{18}F-FDG microPET for future assessment of antimicrobial implant coatings.

Supplementary data

Figure 1 is available at Acta's website (www.actaorthop.org), identification number 6657.

JO participated in the design of the study and performed the initial experiments and data collection, the statistical analysis, and data interpretation, and he also wrote the initial draft of the manuscript. BB participated in the study design, coordination, and interpretation of data, and helped to write the manuscript. TW participated in the study design and coordination and helped to write the manuscript. GW participated in the study design and coordination and helped to write the manuscript.

This study was funded by the Dutch BioMedical Materials program, co-funded by the Dutch Ministry of Economic Affairs. This study is part of the BMM NANTICO Research Project. We thank the employees of the animal facility of the Maastricht University Medical Center for their assistance during this study. We also thank I. Pooters, M. Visser and C. Urbach of the Nuclear Medicine department of the Maastricht University Medical Center for their support during this study, and R. Odekerken for his assistance with the design of the experimental setup. We are very grateful to S. Bout and P. Dijkstra for their overall support during this study.

No competing interests declared.

Acklin Y P, Widmer A F, Renner R M, Frei R, Gross T. Unexpectedly increased rate of surgical site infections following implant surgery for hip fractures: problem solution with the bundle approach. Injury 2011; 42 (2): 209-16.

Alt V, Lips K S, Henkenbehrens C, Muhrer D, Oliveira Cavalcanti M C, Sommer U, Thormann U, Szalay G, Heiss C, Pavlidis T, Domann E, Schnettler R. A new animal model for implant-related infected non-unions after intramedullary fixation of the tibia in rats with fluorescent in situ hybridization of bacteria in bone infection. Bone 2011; 48 (5): 1146-53.

Calhoun J H, Mader J T. Treatment of osteomyelitis with a biodegradable antibiotic implant. Clin Orthop 1997; (341): 206-14.

Cremieux A C, Carbon C. Experimental models of bone and prosthetic joint infections. Clin Infect Dis 1997; 25 (6): 1295-302.

Dale H, Hallan G, Espehaug B, Havelin L I, Engesaeter L B. Increasing risk of revision due to deep infection after hip arthroplasty. Acta Orthop 2009; 80 (6): 639-45.

De Winter F, Vogelaers D, Gemmel F, Dierckx R A. Promising role of ^{18}-F-fluoro-D-deoxyglucose positron emission tomography in clinical infectious diseases. Eur J Clin Microbiol Infect Dis 2002; 21 (4): 247-57.

Geurts J, Chris Arts J J, Walenkamp G H. Bone graft substitutes in active or suspected infection. Contra-indicated or not? Injury (Suppl 2) 2011; 42: S82-6.

Geurts J A, Janssen D M, Kessels A G, Walenkamp G H. Good results in postoperative and hematogenous deep infections of 89 stable total hip and knee replacements with retention of prosthesis and local antibiotics. Acta Orthop 2013; 84 (6): 509-16.

Guhlmann A, Brecht-Krauss D, Suger G, Glatting G, Kotzerke J, Kinzl L, Reske S N. Fluorine-^{18}-FDG PET and technetium-99m antigranulocyte antibody scintigraphy in chronic osteomyelitis. J Nucl Med 1998; 39 (12): 2145-52.

Huang T, Civelek A C, Li J, Jiang H, Ng C K, Postel G C, Shen B, Li X F. Tumor microenvironment-dependent ^{18}F-FDG, ^{18}F-fluorothymidine, and ^{18}F-misonidazole uptake: a pilot study in mouse models of human non-small cell lung cancer. J Nucl Med 2012; 53 (8): 1262-8.

Jones-Jackson L, Walker R, Purnell G, McLaren S G, Skinner R A, Thomas J R, Suva L J, Anaissie E, Miceli M, Nelson C L, Ferris E J, Smeltzer M S. Early detection of bone infection and differentiation from post-surgical inflammation using 2-deoxy-2-[^{18}F]-fluoro-D-glucose positron emission tomography (FDG-PET) in an animal model. J Orthop Res 2005; 23 (6): 1484-9.

Koort J K, Makinen T J, Knuuti J, Jalava J, Aro H T. Comparative ^{18}F-FDG PET of experimental Staphylococcus aureus osteomyelitis and normal bone healing. J Nucl Med 2004; 45 (8): 1406-11.

Koort J K, Makinen T J, Suokas E, Veiranto M, Jalava J, Knuuti J, Tormala P, Aro H T. Efficacy of ciprofloxacin-releasing bioabsorbable osteoconductive bone defect filler for treatment of experimental osteomyelitis due to Staphylococcus aureus. Antimicrob Agents Chemother 2005; 49 (4): 1502-8.

Kurtz S M, Lau E, Ong K L, Carreon L, Watson H, Albert T, Glassman S. Infection risk for primary and revision instrumented lumbar spine fusion in the Medicare population. J Neurosurg Spine 2012; 17 (4): 342-7.

Lankinen P, Lehtimaki K, Hakanen A J, Roivainen A, Aro H T. A comparative ^{18}F-FDG PET/CT imaging of experimental Staphylococcus aureus osteomyelitis and Staphylococcus epidermidis foreign-body-associated infection in the rabbit tibia. EJNMMI research 2012; 2 (1): 41.

Mader J T. Animal models of osteomyelitis. Am J Med 1985; 78 (6B): 213-7.

Makinen T J, Lankinen P, Poyhonen T, Jalava J, Aro H T, Roivainen A. Comparison of ^{18}F-FDG and 68Ga PET imaging in the assessment of experimental osteomyelitis due to Staphylococcus aureus. Eur J Nucl Med Mol Imaging 2005a; 32 (11): 1259-68.

Makinen T J, Veiranto M, Knuuti J, Jalava J, Tormala P, Aro H T. Efficacy of bioabsorbable antibiotic containing bone screw in the prevention of biomaterial-related infection due to Staphylococcus aureus. Bone 2005b; 36 (2): 292-9.

Marsboom G, Wietholt C, Haney C R, Toth P T, Ryan J J, Morrow E, Thenappan T, Bache-Wiig P, Piao L, Paul J, Chen C T, Archer S L. Lung (1) (8)F-fluorodeoxyglucose positron emission tomography for diagnosis and monitoring of pulmonary arterial hypertension. Am J Respir Crit Care Med 2012; 185 (6): 670-9.

Nanni C, Marangoni A, Quarta C, Di Pierro D, Rizzello A, Trespidi S, D'Ambrosio D, Ambrosini V, Donati M, Aldini R, Zanotti-Fregonara P, Grassetto G, Rubello D, Fanti S, Cevenini R. Small animal PET for the evaluation of an animal model of genital infection. Clin Physiol Funct Imaging 2009; 29 (3): 187-92.

Odekerken J C, Arts J J, Surtel D A, Walenkamp G H, Welting T J. A rabbit osteomyelitis model for the longitudinal assessment of early post-operative implant infections. J Orthop Surg Res 2013; 8 (1): 38.

Rodet A. The classic. An experimental study on infectious osteomyelitis. Clin Orthop 1973; (99) (96): 3-4.

Schmitz A, Risse H J, Kalicke T, Grunwald F, Schmitt O. FDG-PET for diagnosis and follow-up of inflammatory processes: initial results from the orthopedic viewpoint. Z Orthop Ihre Grenzgeb 2000; 138 (5): 407-12.

Smeltzer M S, Thomas J R, Hickmon S G, Skinner R A, Nelson C L, Griffith D, Parr T R, Jr., Evans R P. Characterization of a rabbit model of staphylococcal osteomyelitis. J Orthop Res 1997; 15 (3): 414-21.

Stumpe K D, Strobel K. ^{18}F FDG-PET imaging in musculoskeletal infection. Q J Nucl Med Mol Imaging 2006; 50 (2): 131-42.

Stumpe K D, Dazzi H, Schaffner A, von Schulthess G K. Infection imaging using whole-body FDG-PET. Eur J Nucl Med 2000; 27 (7): 822-32.

Temmerman O P, Heyligers I C, Hoekstra O S, Comans E F, Roos J C. Detection of osteomyelitis using FDG and positron emission tomography. J Arthroplasty 2001; 16 (2): 243-6.

Toyama H, Ichise M, Liow J S, Modell K J, Vines D C, Esaki T, Cook M, Seidel J, Sokoloff L, Green M V, Innis R B. Absolute quantification of regional cerebral glucose utilization in mice by ^{18}F-FDG small animal PET scanning and 2-14C-DG autoradiography. J Nucl Med 2004a; 45 (8): 1398-405.

Toyama H, Ichise M, Liow J S, Vines D C, Seneca N M, Modell K J, Seidel J, Green M V, Innis R B. Evaluation of anesthesia effects on [^{18}F]FDG uptake in mouse brain and heart using small animal PET. Nucl Med Biol 2004b; 31 (2): 251-6.

Trampuz A, Zimmerli W. Diagnosis and treatment of infections associated with fracture-fixation devices. Injury (Suppl 2) 2006; 37: S59-66.

Tremoleda J L, Khalil M, Gompels L L, Wylezinska-Arridge M, Vincent T, Gsell W. Imaging technologies for preclinical models of bone and joint disorders. EJNMMI research 2011; 1 (1): 11.

van der Bruggen W, Bleeker-Rovers C P, Boerman O C, Gotthardt M, Oyen W J. PET and SPECT in osteomyelitis and prosthetic bone and joint infections: a systematic review. Semin Nucl Med 2010; 40 (1): 3-15.

Vogely H C, Oosterbos C J, Puts E W, Nijhof M W, Nikkels P G, Fleer A, Tonino A J, Dhert W J, Verbout A J. Effects of hydrosyapatite coating on Ti-6A1-4V implant-site infection in a rabbit tibial model. J Orthop Res 2000; 18 (3): 485-93.

Zhuang H, Alavi A. ^{18}-fluorodeoxyglucose positron emission tomographic imaging in the detection and monitoring of infection and inflammation. Semin Nucl Med 2002; 32 (1): 47-59.

Zimmerli W, Ochsner P E. Management of infection associated with prosthetic joints. Infection 2003; 31 (2): 99-108.